J. of Supercritical Fluids 107 (2016) 486–498

Contents lists available at ScienceDirect

The Journal of Supercritical Fluids

journal homepage: www.elsevier.com/locate/supflu

Supercritical CO_2 sorption kinetics and thymol impregnation of PCL and PCL-HA

Jasna Ivanovic[a,*], Sandra Knauer[b], Alejandra Fanovich[c], Stoja Milovanovic[a], Marko Stamenic[a], Philip Jaeger[b], Irena Zizovic[a], Rudolf Eggers[d]

[a] Department of Organic Chemical Technology, Faculty of Technology and Metallurgy, University of Belgrade, Karnegijeva 4, 11000 Belgrade, Serbia
[b] Eurotechnica GmbH, An den Stücken 55, 22941 Bargteheide, Germany
[c] INTEMA (University Nacional de Mar del Plata, CONICET), Av. J. B. Justo 4302, 7600 Mar del Plata, Argentina
[d] Inst. Thermal Process Engineering, Hamburg University of Technology, Eißendorfer Str. 38, 21073 Hamburg, Germany

ARTICLE INFO

Article history:
Received 17 April 2015
Received in revised form 1 July 2015
Accepted 2 July 2015
Available online 17 July 2015

Keywords:
Polycaprolactone
Polycaprolactone-hydroxyapatite
CO_2 sorption kinetics
High-pressure DSC
Melting point depression
Thymol impregnation

ABSTRACT

The potential of supercritical carbon dioxide ($scCO_2$) processing of polycaprolactone (PCL) and polycaprolactone-hydroxyapatite (PCL-HA) composites for obtaining functional porous scaffolds at moderate temperatures (35–40 °C) was analyzed and quantified. The effect of $scCO_2$ sorption kinetics on the swelling, foam morphology and thermal behavior of the PCL and PCL-HA composites was studied. Sorption isotherms were determined using magnetic suspension balance at 10–30 MPa and 35–40 °C. Influence of the pressure, HA amount (10–20%) and procedure for HA powder preparation on the sorption kinetics was discussed. Supercritical solvent impregnation (SSI) of PCL and PCL-HA with thymol was investigated as environmentally friendly way to produce functional scaffolds with controlled microstructure. Moderately high pressures (13–17 MPa) and 10% of HA were proven to be favorable for creation of the PCL scaffolds with satisfying foam microstructure (mean pore size ~200–300 μm), filler distribution and thymol impregnation yields (12–18%). This was due to the satisfactory high $scCO_2$ solubility (0.25–0.30 g/g) and mass transfer rate (~10^{-10} m^2/s) in the polymer phase as well as its great plasticizing effect ($-\Delta T_m$ = 26.4–27.4 °C). Higher saturation of the polymer phase with $scCO_2$ (0.30–0.55 g/g), filler amount (20%) and thymol solubility in $scCO_2$ (>5.5 g/kg) at pressures above 20 MPa resulted in decreased mass transfer rate and SSI efficiency.

1. Introduction

Bone defects in the oral cavity resulting from trauma, chronic infection, congenital defects, or surgical resection require clinical intervention, most frequently using autologous bone grafting techniques [1]. As consequence, the supply of this graft tissue is a critical limitation in dental field [2]. Tissue engineering approaches using scaffolds alone or in combination with a bioactive agent have the potential to address existing challenges in managing bone loss and increase clinical options for controllable regeneration of intraoral osseous tissues [1,3,4]. Accordingly, lots of attention has been focused on development of new materials and technologies for scaffolds fabrication [5,6]. Semi-crystalline poly(ε-caprolactone) (PCL) has been attractive for fabrication of long term degradable implants with tailorable degradation kinetics due to its biocompatibility, formability, inexpensive production and FDA approval [7]. Mechanical properties and lack of bioactivity of the PCL in terms of osteoconductivity and osteoinductivity are improved by its supplementation with bioceramics such as hydroxyapatite [HA: $Ca_{10}(PO_4)_6(OH)_2$] [2,8]. Therewith, HA is the major inorganic component of teeth, and has been used extensively in dental pulp capping [9]. Fabrication of PCL-HA composites holds a great potential for producing load-bearing parts [10–14].

Main limitations of the conventional techniques for scaffold fabrication (solvent casting with particulate leaching, compression moulding, freeze drying, heat sintering, injection moulding, etc.) include use of large amounts of organic solvents, exposure to high temperatures and difficulty to obtain simultaneously macro, micro- and nanostructural characteristics [5,8]. The unique physical properties of supercritical carbon dioxide ($scCO_2$) provide interesting possibilities for creation of porous 3D scaffolds for the tissue engineering regarding environmental benefits and tuneable properties [5,15]. Predictive knowledge of $scCO_2$ solubility and mass transfer in polymer phase as well as the associated dilation and phase

* Corresponding author. Tel.: +381 11 3303 709.
E-mail address: jasnai@tmf.bg.ac.rs (J. Ivanovic).

http://dx.doi.org/10.1016/j.supflu.2015.07.001
0896-8446/

transitions of the polymer matrix have been of a vital importance in designing supercritical-based generation of new morphologies and porous scaffolds [16–18]. Solubility and diffusivity of $scCO_2$ are significantly affected by the nature of the components, gas concentration and operating pressure and temperature conditions [19,20]. While $scCO_2$ solubility, as maximum amount of the gas dissolved in the polymer without causing phase separation [21], determines the extent of the plasticization effect on the polymer, its diffusivity affects the bubble nucleation and growth phenomena, both influencing final density of the foam [20,22]. It is well known that compressed CO_2 plasticizes semi-crystalline polymers including PCL decreasing their melting point peak toward lower values [15,16,18,23,24]. This phenomenon allows different modifications such as incorporation of additives, formation of foams, polymer blend preparations, polymer bulk graft-modification, etc. [25]. Besides, it is especially advantageous for processing of thermolabile polymers as well as for reducing energy requirements in the case of polymers with higher melting points [26,27].

Over the last two decades a tremendous progress has been made toward improved understanding of the properties of CO_2/polymer solutions in terms of measurement techniques [28] and development of theory or models for specific properties [18,29]. There have been several reports on the measurements of $scCO_2$ sorption in PCL using quartz spring microbalance [22,30], external balance method [31], variable volume cell [16] and magnetic suspension balance (MSB) [17,20]. The main advantages of the magnetic suspension balance over listed methods are high resolution and accuracy of gravimetric measurements in the huge range of applicability due to the physically separated microbalance from the measuring atmosphere by means of a magnetic suspension coupling [32]. There are scanty data on $scCO_2$ sorption kinetics of PCL measured with MSB [17,20]. Solubility of compressed CO_2 in PCL investigated at lower pressures of up to 4.2 MPa and 80–100 °C reached up to 0.055 g_{CO_2}/g_{PCL} [17]. In the same study [17], CO_2 diffusion coefficients were in the range of $4–5 \times 10^{-10}$ m^2/s. Reportedly, higher values for $scCO_2$ solubility in PCL ($0.126 - 0.400\ g_{CO_2}/g_{PCL}$) were determined at higher pressures (10-30 MPa) and temperatures of 30-80 °C by using MSB [20,33]. The $scCO_2$ diffusion coefficients in these studies [20,33] were higher ($\sim 10^{-9} \times 10^{-7}$ m^2/s). To the best of our knowledge there are no available data on $scCO_2$ sorption kinetics of PCL-HA.

Gas induced melting temperature depression of PCL was estimated by optical measurements in a wavelength range from near infrared to visible light, using capillaries, thin polymer discs or films in high pressure view cells or autoclaves for the analysis [16,18,24,34]. Some authors used differential scanning calorimetry (DSC) at ambient pressure to scan foamed samples of PCL or PCL-HA after treatment with $scCO_2$ or previously $scCO_2$ saturated samples to estimate melting point change [16,20,35–37]. In these cases, the pressure in the system may not remain constant during the scan due to the gas desorption, and thus it is not possible to define the thermodynamic state of the system unambiguously [38]. Alternative methods such as high pressure differential scanning calorimetry (HP-DSC) and calorimetric analysis in a pressurized scanning transitiometer enable accurate and direct measurements of thermal properties of polymers in presence of compressed fluids at pressures up to 45 MPa [15,26,39–42]. The advantage of these methods is that the sample and referent crucibles are pressurized. Since the polymer is in equilibrium with the gas phase, problems due to gas desorption encountered with conventional DSC are avoided [41].

Fatal bacterial infections in humans and animals caused by multiresistant pathogenic bacteria have led to increased interest in developing new polymer systems exhibiting antimicrobial activity by a surface modification and/or chemical deposition of synthetic antibiotics [43–47]. Thymol has been recently proven as promising natural antimicrobial [48–50] and antioxidant agent [51,52] with high efficiency in the treatment of inflammatory processes and wound healing [53]. It was proven that thymol efficiently inhibit growth of oral pathogens in the mouth and may reduce dental caries [54,55], whereby thymol based varnishes has been proven to delay bacterial colonization and the development of biofilm [56]. $ScCO_2$ has proved to be a good solvent for thymol [57] and due to its high diffusion ability in organic matter it can be efficiently used for thymol incorporation into different polymer matrices [57–62]. In the available literature there are no data on supercritical solvent impregnation (SSI) of PCL and PCL-HA with thymol.

The present study was aimed to investigate the influence of pressure ($scCO_2$ density) and filler (HA) percentage on the $scCO_2$ sorption kinetics of the PCL and PCL-HA composites. Sorption behavior of the PCL and PCL-HA was correlated to their swelling kinetics, scaffold microstructure, thermal properties and SSI with thymol at moderate temperature (35–40 °C).

2. Materials and methods

2.1. Materials and composite preparation

Granules of the PCL (M_n = 70,000–90,000, CAS 24980-41-4) purchased from Sigma Aldrich (Steinheim, Germany) were used for the experiments. The density of PCL given by manufacturer was 1.145 g/cm^3. Commercial carbon dioxide (99.8% purity) was supplied by Yara GmbH (Brunsbüttel, Germany). Powder of hydroxyapatite (HA) was obtained by a precipitation method as described elsewhere [63]. Starting materials were analytical grade: $CaCO_3$ (99%, PA Cicarelli) as the Ca source and H_3PO_4 (85%, Merck, Country) as the P source. The $CaCO_3$ was thermally treated in an oven (Indef, model 332 p-full) at 1473 K for 2 h to obtain CaO. The solid CaO was first dispersed in ammonium hydroxide (pH = 12) and subjected to conventional mechanical stirring. Subsequently, H_3PO_4 0.5 mol/L was slowly added dropwise into the same beaker at 2 mL/min until reaching the molar ratio of Ca/P = 1.67 with conventional mechanical stirring (M) or ultrasonic irradiation treatment (S). After this step, the reaction mixture was kept at an ageing step during 48 h. Finally, the precipitate was centrifuged and freeze-dried. Two types of filler particles were obtained: HA (M) (mean particle size of 10 μm; specific surface area of 15 m^2/g) and HA (S) (mean particle size of 5 μm; specific surface area of 33 m^2/g) [63]. Nano-HA powder, HA (N) (mean particle size <1 μm; specific surface area of 70 m^2/g [63]) was obtained by the López Macipe [64]. The obtained HA powders were added to the solution of PCL/acetone (1:10) and dispersed with the Ultra Turrax T25 (IKA, Germany) at 20,000 rpm during 10 min. The nominal content of HA added to PCL/acetone solution was 10% or 20% with respect to the PCL weight. The solvent was evaporated at room temperature under a fume hood. The obtained composite films were pelletized and used for the $scCO_2$ processing.

2.2. Swelling and sorption measurements

The setup used for investigation of $scCO_2$ sorption and swelling kinetics of the PCL and PCL-HA is given in Fig. 1. The experiments were carried out in the pressure range of 10–30 MPa and at 35 °C or 40 °C. The main part of the setup (Fig. 1) is the magnetic suspension balance (MSB) (Rubotherm GmbH) connected to the high pressure view cell (Eurotechnica GmbH, Bargteheide, Germany). Maximum operating pressure and temperature of this system is 35 MPa and 120 °C, respectively. A high pressure view cell provided with the CCD camera enabled visual monitoring and quantification of swelling extent of the PCL and PCL-HA in a presence of $scCO_2$. The volume changes of the samples exposed to $scCO_2$ over 24 h were monitored by recording the two-dimensional projection of

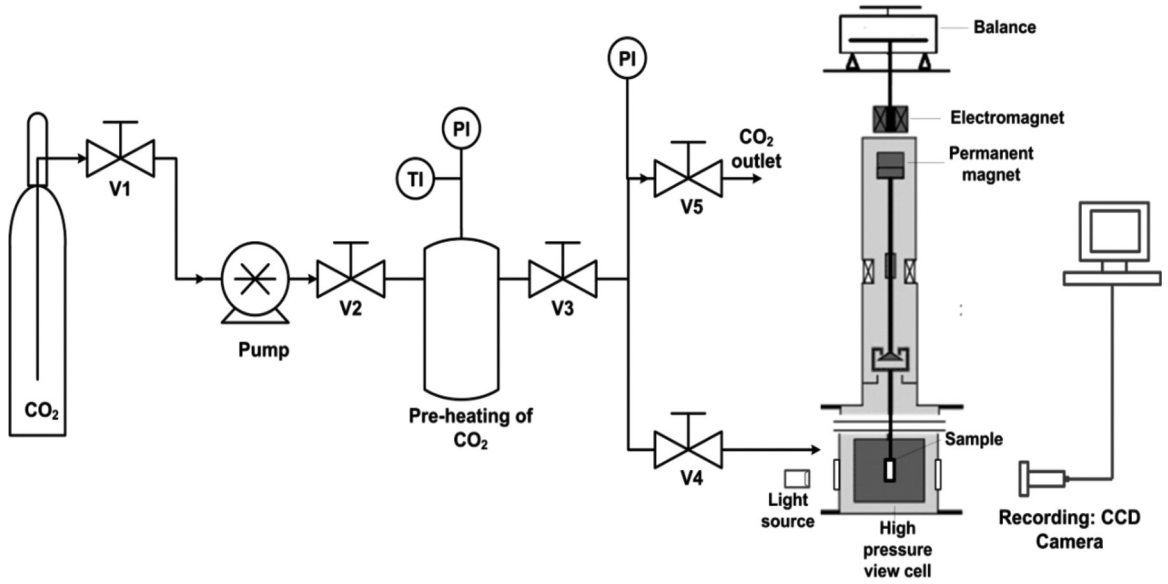

Fig. 1. Experimental set-up for the gravimetric measurement of CO_2 sorption.

the rotationally symmetric sample with time using the IC Capture 2.1 software. All the samples used for the swelling measurements were disc shaped. The disc's diameter was same as diameter of the glass container (13 ± 0.5 mm = const.). The initial height of the PCL and PCL-HA discs was 3.3 ± 0.2 mm and 2.0 ± 0.2 mm, respectively. The change of the sample's dimension (height, L) due to swelling was determined by image processing with Image-Pro Plus 6.0.

Relative volume change denoted as swelling extent (S_w) was calculated using the following equation:

$$S_w\,(\%) = \frac{V_t - V_o}{V_o} \times 100 = \left(\frac{L}{L_o} - 1\right) \times 100 \tag{1}$$

where V_0 is the volume of polymer (or composite) at ambient conditions at $t = 0$, V_t is the volume of swollen polymer (or its composite) at $t > 0$ and given pressure and temperature, L and L_0 are the levels of polymer molded in the glass beaker at the time t and given pressure/temperature and at the ambient conditions, respectively.

The sample placed in the high pressure view cell is coupled to the balance by means of a contactless magnetic suspension coupling [32]. An electromagnet attached to the bottom of the balance lifts the so-called suspension magnet, which consists of a permanent magnet, a sensor core and a measuring load decoupling cage. Glass containment with the sample inside is connected to the permanent magnet inside the high pressure view chamber which on its turn is pressurized with CO_2 pre-heated (Fig. 1) to the same temperature as inside of the balance. The magnetic suspension balance is placed inside a heating air bath. The time dependant mass of the polymer sample (w_t) is detected via a magnetic coupling by a microbalance on the outside of the pressure chamber and recorded by a PC which also controls the magnetic coupling. The recorded balance readings must be corrected for the change in buoyancy that occurs due to swelling according to Eq. (2) [65]. The mass gain (M_t) under pressure can be determined by knowing the exact volume of the sample at a certain time t (V_t), the initial weight of the sample at atmospheric pressure (w_0) and the density of CO_2.

$$M_t = \left(w_t - V_t \rho_{CO_2}\right) - w_0 \tag{2}$$

In order to quantify the mass transfer of the gas within the polymer, the apparent diffusion coefficient was determined by fitting the experimental sorption curves with the one-dimensional Fick's law for non-stationary diffusion by Crank [66] solved for spherical PCL particles using Eq. (3) and for thin PCL-HA composite films using Eq. (4). The PCL sphere ($d = 6$ mm) and PCL-HA films ($L = 2$ mm) were used for the foaming tests. Mass of the test samples was 0.127 ± 0.0062 g.

$$\frac{\Delta w_{CO_2}(t)}{\Delta w_{CO_2}(t=\infty)} = 1 - \frac{6}{\pi^2}\sum_{n=1}^{\infty}\frac{1}{n^2}\exp\left[\frac{-Dn^2\pi^2 t}{r^2}\right] \tag{3}$$

[20]

$$\frac{\Delta w_{CO_2}(t)}{\Delta w_{CO_2}(t=\infty)} = 1 - \frac{8}{\pi^2}\sum_{n=1}^{\infty}\frac{1}{(2n+1)^2}\exp\left[\frac{-D(2n+1)^2\pi^2 t}{4L^2}\right] \tag{4}$$

[67]where r is the sphere radius and L is the thickness of the film.

2.3. Foam characterization

Foams were obtained by 24 h exposure of the PCL and PCL-HA samples to $scCO_2$ at 10–30 MPa and 35 °C or 40 °C and subsequent decompression at 0.5 MPa/min [15,20]. Pore morphology of the PCL and PCL-HA foams was investigated by the field emission scanning electron microscopy (FE-SEM, Mira3 XMU TESCAN a.s., Brno, Czech Republic) operated at the accelerating voltage of 10 kV. The samples of PCL and PCL-HA foams were coated with a thin layer of Au/Pd (85/15), using a sputter coater (POLARON SC502, Fisons Instruments, Ipswich, UK) prior to the analysis. Density of the scaffolds was determined by using a Mettler analytical balance (AE100) with a density kit. Foam density (ρ_{foam}) was calculated using Eq. (5) according to the previously described procedure [68].

$$\rho_{foam} = \frac{\rho_{H_2O} \times w_1}{w_1 + w_2 - w_3} \tag{5}$$

where w_1 is the mass of sample, w_2 is the mass of picnometer and water, w_3 is the mass of glass with water and the sample. Density of water at 23.3 ± 0.5 °C is 997.3 ± 0.2 kg/m^3. Porosity was calculated using the following equation [35]:

$$\varepsilon\,(\%) = \left(1 - \frac{\rho_{foam}}{\rho_{PCL}}\right) \times 100 \tag{6}$$

2.4. High pressure-differential calorimetry (HP-DSC)

The scheme of the setup for the high pressure differential scanning calorimetry (HP-DSC) measurements of thermal properties of

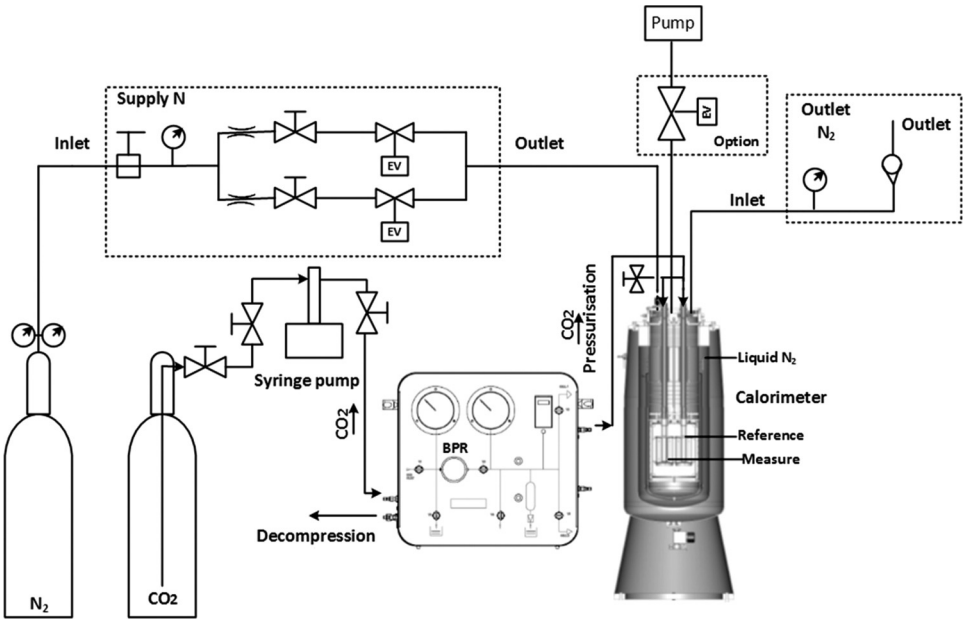

Fig. 2. Setup for the high pressure differential scanning calorimetry (HP-DSC).

the polycaprolactone (PCL) and polycaprolactone-hydroxyapatite (PCL-HA) composites is presented in Fig. 2. The low temperature Tian-Calvet differential scanning calorimeter BT2.15 (Setaram, France) which has an operating temperature range of 77 K to 473 K was used for measurements. The BT 2.15 is equipped with an integrated liquid nitrogen cooling loop for operation at sub-ambient temperatures.

The DSC is coupled with a gas control panel that can withstand maximum pressures of 20 MPa.

Standard stainless steel vessels ($V = 12\,cm^3$, $p_{max} = 0.5$ MPa, $T_{max} = 220\,^{\circ}C$) and intermediate bottom stainless steel vessels ($V = 8.5\,cm^3$, $p_{max} = 0.5$ MPa, $t_{max} = 220\,^{\circ}C$) were used for the measurements at atmospheric conditions. High pressure crucibles made of Inconel 625 ($V = 3.6\,cm^3$, $p_{max} = 60$ MPa, $T_{max} = 500\,^{\circ}C$) were used for measurements at higher pressures in the range of 4.6–17.0 MPa. The sample was heated at a rate of 0.10 °C/min over a temperature range of room temperature 25 °C to 85 °C. An empty, hermetically sealed stainless steel pan was used as a reference. Melting point and enthalpies of indium were used for temperature and heat capacity calibration. Fusion enthalpy (ΔH_m) was calculated using Calisto Data Acquisition software (Version 1.071). The crystallinity (χ_c) of PCL samples was determined using a heat of fusion value (ΔH_m^0) of 135.31 J/g [69] for 100% crystalline PCL according to the following equation:

$$\chi_c\,(\%) = \frac{\Delta H_m}{\Delta H_m^0} \times 100 \tag{7}$$

2.5. Supercritical solvent impregnation (SSI) of thymol

The SSI of PCL and PCL-HA with thymol was performed in a high-pressure view chamber (Eurotechnica GmbH) [57] using a static method previously described elsewhere [60,62]. Thymol was placed at the bottom of the vessel in a glass container with a filter on its top to avoid possible splashing during decompression. Polymers were placed in a porous basket above the thymol. The $scCO_2$ was introduced from the top of the previously heated vessel and the pressure was elevated. The experiments were carried out at pressures of 10, 13, 17, 20 and 30 MPa, and at temperatures of 35 °C or 40 °C. The impregnation time was 2 h. The mass ratio of PCL or (PCL-HA)/thymol was 1:1. Applied decompression rate was 0.5 MPa/min [20]. Impregnated mass of thymol (m_T) was determined gravimetrically by measuring the impregnated sample. The impregnation yield (I) of PCL or PCL-HA was calculated from the following equation:

$$I\,(\%) = \frac{m_T}{m_T + m_P} \times 100 \tag{8}$$

where m_P is the polymer mass at the beginning of the process.

The efficiency of the SSI of PCL and PCL-HA with thymol was described with the partition coefficient, K_c [65], the ratio of the thymol mass concentration in fluid ($q_T^{CO_2}$) and polymer phase (q_T^{PCL}) for the given time of impregnation according to Eqs. (9), (10)and (11), respectively.

$$K_c = \frac{q_T^{PCL}}{q_T^{CO_2}} \tag{9}$$

$$q_T^{CO_2}(g/kg) = \frac{C_T^{CO_2} \times 1000}{\rho_{CO_2}} \tag{10}$$

$$q_T^{PCL} = \frac{m_T}{m_P} \tag{11}$$

Thymol concentration in $scCO_2$ was determined using a static method in a high-pressure view chamber (Eurotechnica GmbH) previously described in detail in [57]. Solubility of thymol in $scCO_2$ was experimentally determined at temperatures of 35 °C and 40 °C, and pressures ranged from 10 MPa to 30 MPa ($scCO_2$ density range of 630–911 kg/m^3) for 2 h.

2.6. Statistics

All the experiments were performed in triplicate. The mean value and standard deviation were calculated using the OriginPro 8 software (OriginLab Corporation, Northampton, MA, USA). A one-way ANOVA (analysis of variance) method followed by post hoc Tukey's test was used to evaluate the significant difference among various treatments with the criterion of $p \leq 0.05$. Pearson product moment correlation is used to assess linear correlation coefficients (r) among means.

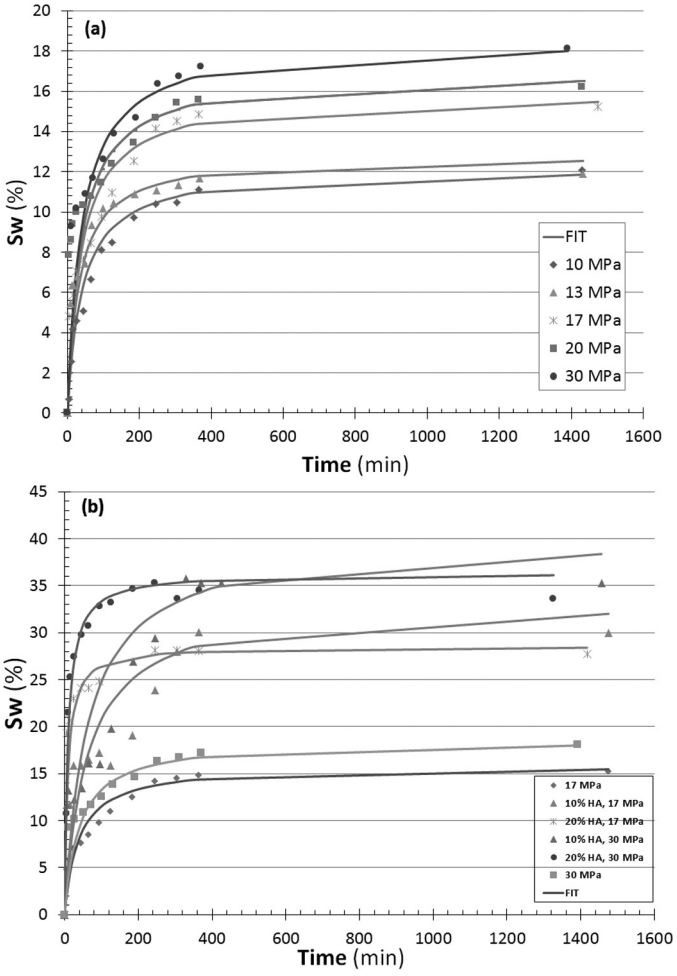

Fig. 3. Effect (a) of the pressure on the neat PCL swelling, and (b) HA amount on PCL-HA swelling.

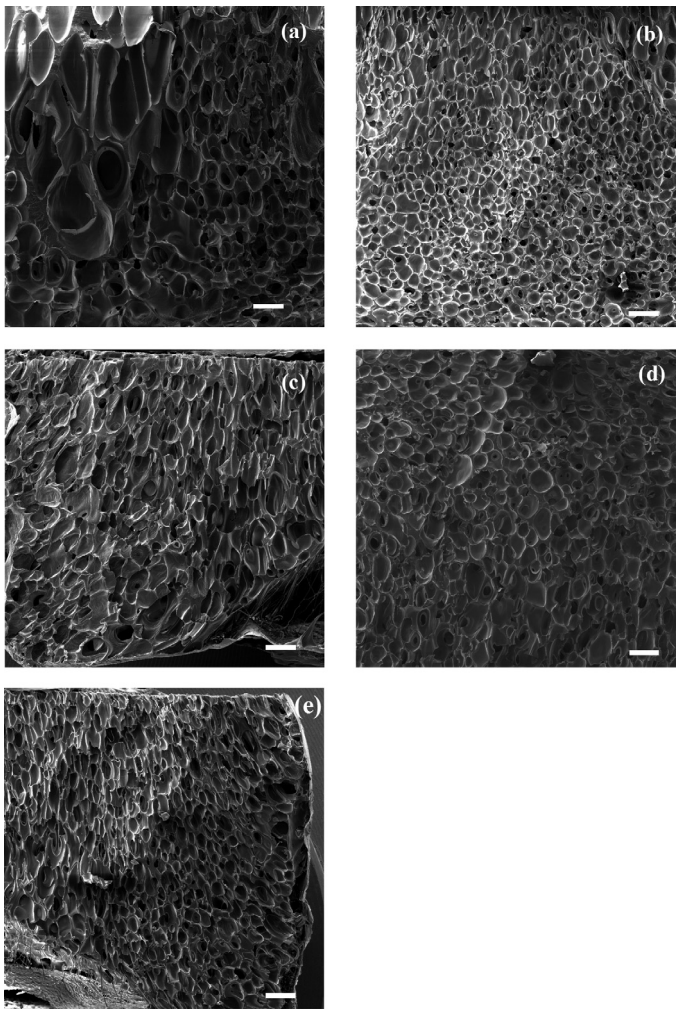

Fig. 4. Pressure effect on microstructure of the PCL foams obtained at 40 °C: (a) 10 MPa, (b) 13 MPa, (c) 17 MPa, (d) 20 MPa, and (e) 30 MPa (scale bar = 500 μm).

3. Results and discussion

3.1. Pressure and filler amount effect on the swelling kinetics and foam morphology

Optical experiments in the high pressure view cell were carried out prior to the sorption experiments to visualize and quantify the PCL and PCL-HA relative volume variation (swelling extent, S_w). Swelling curves in Fig. 3 represent the change of the S_w regarding the initial volume of the polymer or composite (V_0) within time during exposure to $scCO_2$ at 10–30 MPa and 35 °C or 40 °C. The swelling isotherms (Fig. 3) were fitted ($S_w = (\Delta V/100)/V_0 = 1/(A + 1/Bt)$) to estimate A and B coefficients (Table 1) which were used further for buoyancy correction to determine actual volume and mass of the adsorbed $scCO_2$ (V_t and w_t) given in Eq. (2). The effect of the pressure (Fig. 3a) and amount of HA (M) (Fig. 3b) in the PCL on the swelling extent was analyzed. Pressure increase from 10 MPa to 30 MPa strongly influenced volume variation resulting in 40% higher swelling extent of the pure PCL at 40 °C. The biggest change of the PCL swelling rate within the first 30 min of the exposure to $scCO_2$ was observed for the pressure range of 10–17 MPa, while it became insignificant at higher pressures (Fig. 3a). Relative volume's variation observed after 24 h was three times smaller (0.15% per MPa) at pressures above 17 MPa than in the lower pressure range (0.51% per MPa).

Swelling extent of the PCL-HA composites determined after 24 h was two times higher in comparison to the pure PCL at same conditions (Fig. 3b). The lower extent of swelling of the composite with 20% HA in comparison to the one with only 10% could be due to the increased amount of the filler which doesn't change its volume during $scCO_2$ sorption and acts like an obstacle to the mass transfer and gas sorption [70].

The influence of the pressure ($scCO_2$ density) and HA amount on the PCL and PCL-HA foam microstructure was analysed by SEM. Porous microstructure was observed in all the cases (Figs. 4 and 5). The average pore diameter, foam density and porosity are given in Table 2. SEM images of the PCL foams obtained at different pressures are shown in Fig. 4. Positive effect of pressure increase on the pore morphology was the most noticeable in the lower pressure range, from 10 MPa to 13 MPa. The pressure increase from 10 MPa to 13 MPa resulted in creation of the foam with 35% smaller average pore diameter and more homogenous structure (Fig. 4, Table 2). The PCL foams obtained at 13 MPa and higher pressures had a homogeneous pore distribution (Fig. 4), satisfactory porosity (72–79%) [15] and mean pore diameter (~300 μm) (Table 2) which is in accordance with the requirements for scaffolds to be used in tissue engineering for proper bone ingrowth and vascularization [71].

SEM images of the PCL-HA foams are presented in Fig. 5. The average pore diameter of PCL-HA foams was smaller (31–72%) in comparison to the PCL foams obtained at same conditions (Table 2). This could be due the higher $scCO_2$ uptake of PCL-HA composites as a consequence of a lower degree of crystallinity, especially in the case of PCL-HA (10S) and PCL-HA (20M). All the PCL-HA foams

Table 1
Coefficients for buoyancy correction.

PCL p (MPa)/T (°C)	A (–)	B (min^{-1})	PCL-HA (M) p (MPa)/T (K)/%HA	A (–)	B (min^{-1})
10/40	0.082	0.30	17/35/10	0.03	0.55
13/40	0.078	0.40	17/35/20	0.035	3.50
17/40	0.063	0.42	30/40/10	0.025	0.65
20/40	0.059	0.45	30/40/20	0.0275	4.00
30/40	0.047	0.47			

Table 2
Foam properties: mean pore diameter (d_{avg}), foam density (ρ_{foam}) and porosity (ε).

p (MPa)	T (°C)	HA (%)	d_{avg} (μm)	ρ_{foam} (kg/m^3)	ε (%)
PCL					
10	40	0	462 ± 190^{a}	369.1 ± 25.2^{a}	67.8 ± 2.2^{a}
13	40	0	294 ± 62^{a,b}	244.6 ± 34.2^{b}	78.6 ± 3.0^{b}
17	40	0	310 ± 100^{a,b}	285.1 ± 23.9^{b}	75.1 ± 2.1^{b}
20	40	0	326 ± 90^{a,b}	259.5 ± 16.7^{a}	77.3 ± 1.5^{a}
30	40	0	297 ± 37^{a,b}	324.2 ± 17.3^{a,b}	71.7 ± 1.5^{a,b}
PCL-HA (M)					
17	35	0	296 ± 78^{a,b}	275.5 ± 1.5^{b}	75.9 ± 0.09^{b}
17	35	10	204 ± 75^{b}	295.6 ± 26.1^{a,b}	74.2 ± 2.3^{a,b}
30	40	10	144 ± 23^{b}	282.7 ± 4.7^{a,b}	75.3 ± 0.4^{a,b}
17	35	20	135 ± 33^{b}	324.4 ± 8.1^{a,b}	71.7 ± 0.7^{a,b}
30	40	20	187 ± 43^{b}	323.0 ± 1.8^{a,b}	71.8 ± 0.2^{a,b}
PCL-HA (N)					
17	35	10	176 ± 31^{b}	306.5 ± 4.4^{a,b}	73.2 ± 0.4^{a,b}
30	40	10	148 ± 26^{b}	286.5 ± 28.6^{a,b}	75.0 ± 2.5^{a,b}
PCL-HA (S)					
17	35	10	84 ± 25^{b,c}	288.1 ± 67.1^{a,b}	74.8 ± 5.9^{a,b}
30	40	10	121 ± 41^{b}	306.3 ± 57.6^{a,b}	73.3 ± 5.0^{a,b}

Values represent the means ± standard deviation; n = 3. Means with different superscripts in the same column are significantly different at 0.05 level.

(10–20% of HA) had homogenous pore distribution. Foams of PCL-HA (10S) and PCL-HA (20M) composites obtained at lower pressure (17 MPa) had smaller pores then those produced at 30 MPa. At higher pressures and high saturation of the polymer with gas, the excess of the filler particles or their weak interaction with polymer matrix along with the increased contribution of hydrostatic pressure (free volume in the polymer is decreased) could be an additional obstacle to the mass transfer. This could also explain the reduced swelling of PCL-HA with 20% of HA compared to the one with 10% of HA at the same pressure (Fig. 3b). Density of the PCL and PCL-HA foams was in the range of 245–369 kg/m^3. Previously reported density of PCL and PCL-HA foams with 5% of HA nanoparticles obtained by foaming at 10 to 20 MPa and 37–40 °C was in the range of 200–530 kg/m^3 [35]. Porosity of the obtained foams in this study was in the range of 68–79%. Salerno et al. [14] have recently reported similar porosities of PCL and PCL-HA foams with 5–10% of HA micro- and nanoparticles (77–81%) obtained by foaming at 20 MPa and 40–45 °C.

In order to understand and rationalize the effect of pressure and filler on the swelling and foam morphology, $scCO_2$ solubility (sorption kinetics) and diffusivity were further investigated.

3.2. Sorption kinetics and diffusion coefficients

Experimental results of the $scCO_2$ sorption in the PCL ($q_{CO_2} = w_{CO_2}/w_{PCL}$) in the pressure range of 10–30 MPa and constant temperature are presented in Fig. 6. The solubility of $scCO_2$ denoted as $q_{CO_2}(t \to \infty) = q^{\infty}_{CO_2}$ in PCL (Table 3) was positively affected by pressure increase at constant temperature (40 °C). Accordingly, the best $scCO_2$ solubility in PCL was observed at 30 MPa (0.392 g_{CO_2}/g_p). The highest sorption rate was observed at pressure of 17 MPa and higher in the first 20–30 min. This was in accordance with the previous observation of plasticizing profile of PCL in high pressure view cell at moderate temperatures 35–40 °C [20]. The mentioned study [20] showed that PCL sample was completely plasticized after 30 min at 17 MPa without shape deformation, while at higher pressures (20 MPa) its shape is changed after 20 min. Corresponding diffusion coefficients (D) determined by fitting the experimental sorption isotherms with one-dimensional Fick's second law are given in Table 3.

Pressure increase up to 20 MPa had a positive effect on the diffusion of $scCO_2$ in PCL. The decreasing diffusion coefficient at higher pressures (30 MPa, Table 3) can be explained as follows. The variation of the diffusion coefficient is affected by both, the plasticizing effect of compressed CO_2 and by the hydrostatic effect of pressure. During $scCO_2$ sorption, the molecules in the polymer–gas system are rearranged toward a new equilibrium conformation. At lower pressures, i.e. in the presence of a smaller amount of $scCO_2$ in polymer (Table 3), the plasticizing effect of $scCO_2$ is reflected in a higher mobility of the polymer chains which results in increased values of the diffusion coefficient. However, at high pressures, when there is a higher concentration of $scCO_2$ in the polymer, the hydrostatic pressure may play an important role by reducing the available free volume and leading to decreased diffusivity [40,72].

The effect of the type or amount of HA powder on the $scCO_2$ sorption kinetics was investigated at moderately high (17 MPa) and high pressure (30 MPa). Sorption isotherms are presented in Fig. 7. $ScCO_2$ solubility in PCL-HA composites and corresponding diffusion

Table 3
$ScCO_2$ solubility ($q^{\infty}_{CO_2}$) and diffusion coefficients (D) for PCL.

p (MPa)	$q^{\infty}_{CO_2}$ $\left(g_{CO_2}/g_p\right)$	D (m^2/s)[10]
10	0.208 ± 0.0014	1.15 ± 0.050
13	0.247 ± 0.00066	2.10 ± 0.10
17	0.305 ± 0.00060	2.45 ± 0.050
20	0.330 ± 0.0017	2.85 ± 0.050
30	0.392 ± 0.0063	1.90 ± 0.10

Values represent the means ± standard deviation; n = 3. All the means in each column differ significantly at the 0.05 level.

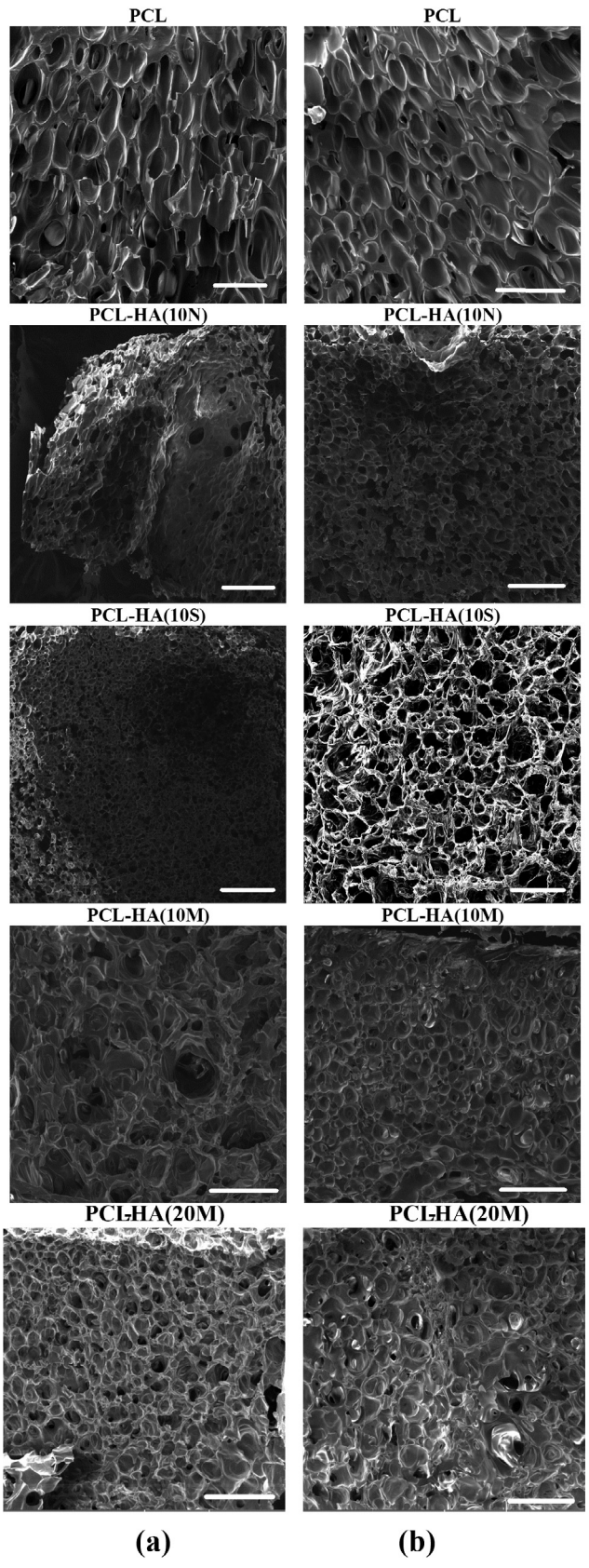

Fig. 5. SEM images of the PCL and PCL-HA foams obtained at (a) 17 MPa and 35 °C, and (b) 30 MPa and 40 °C (scale bar = 500 μm).

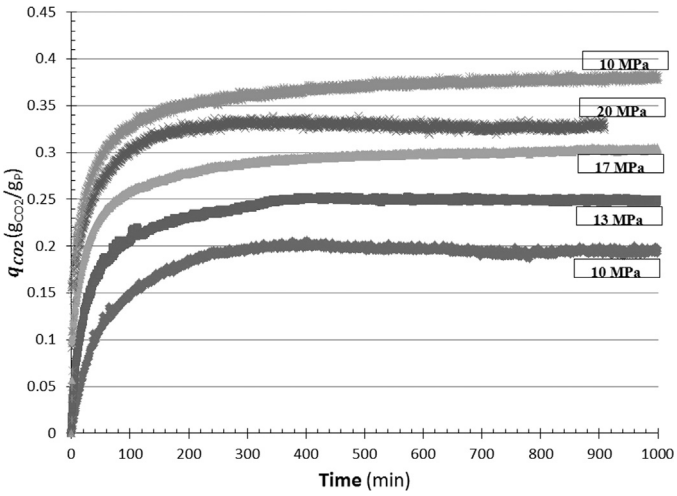

Fig. 6. Pressure effect on the $scCO_2$ sorption of the neat PCL at 40 °C.

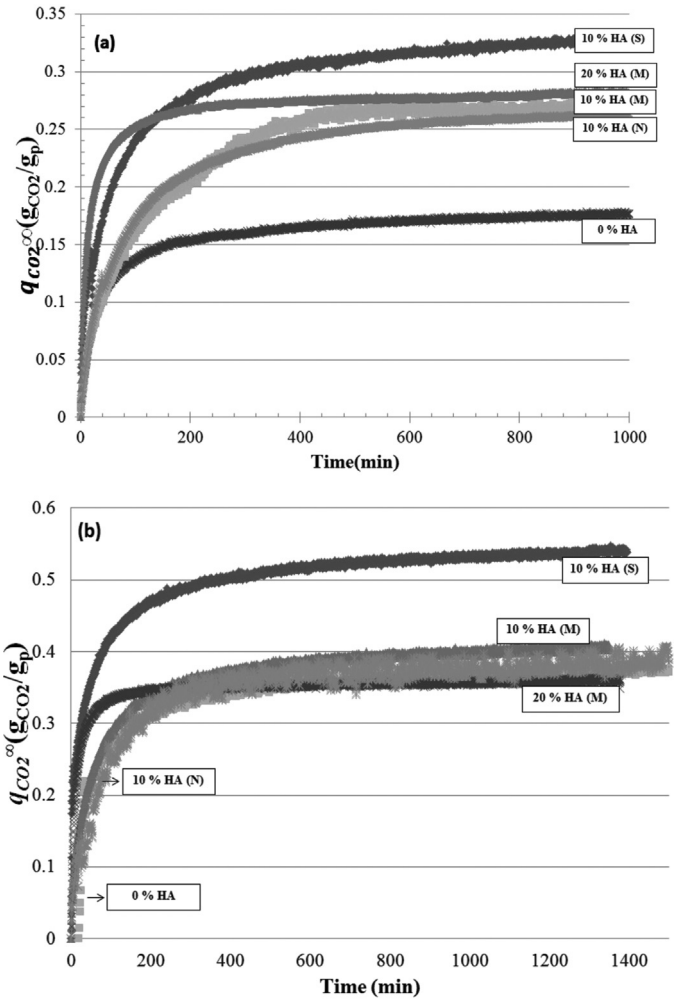

Fig. 7. Influence of HA content and its preparation (particle size) on the CO_2 sorption in the neat PCL and PCL-HA at (a) 17 MPa and 35 °C, and (b) 30 MPa and 40 °C.

Table 4
$ScCO_2$ solubility ($q^{\infty}_{CO_2}$) and diffusion coefficients (D) for PCL-HA.

%HA	$q^{\infty}_{CO_2}$ $\left(g_{CO_2}/g_p\right)$	D (m^2/s) 10^{10}
p (MPa)/t (°C)	17/35	
0	0.185 ± 0.00046[a]	1.20 ± 0.10[a]
10(N)	0.239 ± 0.00040[b]	0.548 ± 0.26[b]
10(M)	0.234 ± 0.0019[c,b]	0.465 ± 0.00010[b,a]
20(M)	0.227 ± 0.00034[c]	3.01 ± 0.10[c]
10(S)	0.295 ± 0.00091[d]	1.32 ± 0.0010[a]
p (MPa)/t (°C)	30/40	
0	0.392 ± 0.0062[e]	1.90 ± 0.10[d]
10(N)	0.392 ± 0.0039[e]	0.544 ± 0.34[b]
10(M)	0.360 ± 0.0018[f]	0.965 ± 0.00020[a,b]
20(M)	0.285 ± 0.0020[g]	3.62 ± 0.18[e]
10(S)	0.494 ± 0.0016[h]	6.40 ± 0.37[f]

Values represent the means ± standard deviation; $n = 3$. Means with different superscripts in the same column are significantly different at 0.05 level.

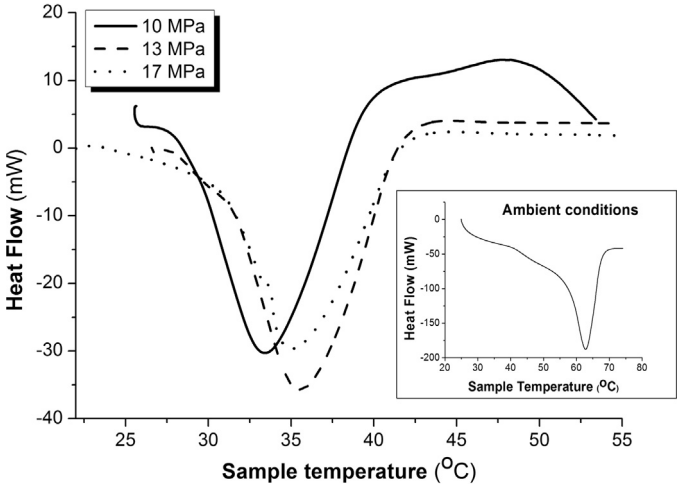

Fig. 8. HP-DSC curves for the PCL exposed to compressed CO_2.

coefficients are given in Table 4. PCL-HA composites are heterogeneous materials composed of a dispersed phase, the filler, and a continuous phase, the polymer. $ScCO_2$ solubility is affected by the presence of the filler in two ways, depending on its integration in the polymer matrix [70]. Intimate contact and even dispersion of the filler in the matrix (the polymer 'wets' the filler particles) may result in a decreased free volume in the polymer which is otherwise available to the dissolving gas. Consequently, sorption is decreased. In the case of uneven dispersion of the filler throughout the matrix, air gaps may appear in the composite structure which may lead to increased solubility [67,70] and diffusivity [73].

Similar or lower $scCO_2$ solubility and lower values for diffusion coefficients observed for PCL-HA (10N) and PCL-HA (10M) indicated better contact of the filler particles and polymer matrix and more even dispersion of HA crystallites. For the PCL-HA (10N) the diffusion coefficient remained constant at increasing pressure indicating better contact of the HA (N) powder with the polymer matrix in comparison to the HA (M) powder. This might be due to the smaller mean particle size (1 μm) and higher specific area of the HA (N) powder (70 m^2/g) in comparison to HA (M) powder (10 μm; 15 m^2/g). On the other side, the highest solubility and diffusion coefficient of $scCO_2$ were observed for the PCL-HA (S) and PCL-HA (20M) samples (Fig. 7) indicated less intimate contact of the filler particles with polymer matrix. Values for the solubility and diffusion coefficient of $scCO_2$ in the case of PCL-HA (20M) were higher at lower pressure (17 MPa) than at higher pressure (30 MPa) in comparison to the virgin polymer at the same conditions. The following explanation could be given. Higher solubility at lower pressure might be due to the lower degree of crystallinity in the case of composite. On the other hand, at higher pressure the hydrostatic pressure contributes to a slower mass transport along with increased amount of HA particles that act as additional obstructions, hindering chain mobility. In order to explain and quantify the effect of $scCO_2$ solubility on the thermal behavior of the tested materials, HP-DSC was applied for in situ determination of the melting temperature range shift and degree of crystallinity.

3.3. Thermal behavior–melting point depression rate and crystallinity

The effect of the pressure and HA percentage on the thermal behavior of neat PCL and PCL-HA was investigated using HP-DSC. Corresponding HP-DSC curves for the neat PCL are presented in Fig. 8. Thermal properties of PCL and PCL-HA determined by HP-DSC are given in Table 5. Melting temperature (T_m) of the neat PCL at atmospheric conditions was 62.5 °C. In this study, a shift of the PCL melting peak (ΔT_m) toward lower values increased with the pressure, reaching its maximum at 10 MPa (−28 °C) (Table 5). The observed rate of depression of melting peak (dT_m/dP) for the pressure range of 0.1–10 MPa was −2.86 ± 0.30 °C/MPa. Previously reported rates of melting point depression of the PCL exposed to $scCO_2$ determined by optical measurements for the same pressure range, 0.1–10 MPa was ranged from −2.41 to −2.75 °C/MPa [16,18]. Reportedly, solubility of $scCO_2$ in most molten polymers at moderate pressures (1 MPa < p < 8 MPa) increases rapidly and almost linearly with pressure increase [18]. Beyond a certain pressure, the solubility of CO_2 increases only by a very small extent even at a larger pressure increase, resulting in an almost vertical pressure vs. mol fraction of CO_2 equilibrium line [18,34,74].

The minimum melting temperature has been explained as a consequence of the balanced CO_2 dissolution in the polymer phase, which tends to reduce the melting temperature, and hydrostatic pressure, which tends to shift melting toward higher temperatures [34]. Reportedly, for PCL the hydrostatic pressure effect starts to prevail at pressures in the range of 10–20 MPa [34,75]. This was also evident in this study in accordance to the change of the melting peak toward higher values at pressures above 10 MPa (Fig. 8, Table 5). Besides the hydrostatic pressure effect, shifting of the melting peak toward higher values, has been recently explained by two more phenomena: lamellar thickening due to the enhanced chain mobility upon dissolution of CO_2 in the polymer which leads to crystallization (at p > 3.6 MPa) [18,31], and the possible extraction of the low molecular weight fractions (oligomers) that sometimes act as plasticizers inside the polymer matrix by CO_2 [34].

The presence of 10–20% of HA in the PCL resulted in 5.0–5.5% higher melting peak shift in comparison to the virgin polymer at the same pressure (17 MPa) (Table 5). PCL-HA (10N) and PCL-HA (10M) samples exhibited similar thermal behavior as PCL, including melting peak shift, fusion enthalpy and degree of crystallinity (Fig. 8, Table 5). This supported previous assumptions on good dispersion of the filler and its intimate contact with the polymer matrix, especially in the case of PCL-HA (10N) which had the narrowest melting range (2.27 °C). The HP-DSC analysis confirmed the previously assumed lower degree of crystallinity of PCL-HA (10S) and PCL-HA (20M) based on the higher sorption rate (Fig. 7).

The Clapeyron equation with a modest modification was used to describe both the slope and the extent of the linearly decreasing melting peak of the neat PCL. Neglecting the contributions of the crystalline and polymer-rich fluid phase to the molar volumes and

Table 5
Thermal properties of PCL and PCL-HA determined by HP-DSC: melting peak shift (ΔT_m–P), melting enthalpy (ΔH_m), crystallinity (χ_c) and melting range (T_i–T_f) of PCL and PCL-HA exposed to the compressed CO_2.

p (MPa)	%HA	$-\Delta T_m$ (°C)	ΔH_m (J/g)	χ_c (%)	T_i–T_f (°C)
PCL					
0.1	0	0	72.69	57.09	56.30–67.50
4.6		16.97	35.82	26.47	39.96–49.93
5.5		19.28	31.32	23.14	37.33–47.79
9		26.84	47.61	35.18	30.47–41.37
10		28.11	46.01	34.00	28.78–39.46
13		26.94	48.83	36.09	30.59–41.54
17		27.38	53.57	39.59	32.94–41.43
PCL-HA					
17	10N	26.66	42.90	31.70	33.6–35.87
17	10M	26.37	41.51	30.68	30.76–38.51
17	10S	27.37	39.40	29.12	30.44–36.33
17	20M	26.88	35.38	26.15	32.03–39.07

$-\Delta T_m$–P—the difference between melting peak at certain pressure ($p > p_{atm}$) and melting peak at atmospheric pressure; T_i–T_f—melting range (T_i—onset temperature, T_f—offset temperature).

enthalpies in the PCL–CO_2 system, at low pressures, the Clapeyron equation is reduced to the following equation [18]:

$$\frac{dT_m}{dP} \approx \frac{-Tm^2 R k_H}{\Delta H_u^{fus}} \quad (12)$$

where R is the universal gas constant, and k_H is the Henry's law constant for sorption of a compressed fluid into a molten polymer. Molar heat of fusion of the crystalline polymer unit was calculated as $\Delta H_u^{fus} = \Delta H_m^0 \cdot M_w^u$ while the compressibility factor (Z) was assumed to be near unity [18,69]. A literature value for the heat of fusion of 100% crystalline PCL (ΔH_m^0) is 135.31 J/g [15,69]. M_w^u is the molar weight of the Kuhn unit. Graphical presentation of experimental results from Table 5 and their fitting are presented in Fig. 9.

It can be seen that the pressure dependence of T_m is practically linear in the range of 0.1 MPa to 10 MPa. The slope obtained by the linear fitting of the experimental data for the neat PCL in the low pressure area was −2.86 K/MPa. This is in fair agreement with experimental results of Lian et al. [18] (−2.41 K/MPa) and Karimi et al. [16] (−2.75 K/MPa) obtained for PCL in the same pressure range. When there are available experimental data on T_m–P dependency, Eq. (10) can be used to evaluate the k_H value at ambient conditions. Adopting the literature value for ΔH_u fusion [15], and the Kuhn length for PCL of 92 Da, as suggested by Lian et al. [18],

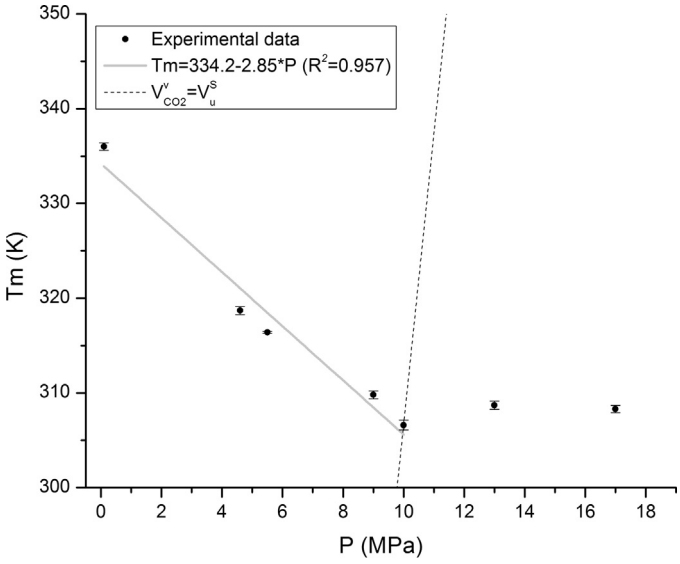

Fig. 9. Experimental results for T_m–P dependency for PCL-CO_2 system: (−) linear fit of the low pressure area, (—) line corresponds to CO_2 isochor which matches the molar volume of the crystalline solid (PCL).

Table 6
Solubility of thymol in CO_2 ($q_T^{CO_2}$), thymol fraction in polymer (q_T^{PCL}), thymol impregnation yields (I) and partitioning coefficients (K_c).

	T (°C)	ρCO_2 $\left(kg/m^3\right)$	$c_T{}^{CO_2}$ $\left(kg/m^3\right)$	$q_T^{CO_2}$ (g/kg)[a]	q_T^{PCL} (kg/kg)	I (%)	K_c
PCL p (MPa)							
10	40	630	2.07 ± 0.13[a]	3.29 ± 0.00021[a]	0.310 ± 0.0012[a]	23.7 ± 0.12[a]	94.4 ± 0.35[a]
13	40	744	3.12 ± 0.053[b]	4.19 ± 0.000071[b]	0.225 ± 0.00085[b]	18.4 ± 0.085[b]	53.8 ± 0.20[b]
17	40	809	4.30 ± 0.29[c]	5.31 ± 0.00035[c]	0.192 ± 0.00088[c]	15.8 ± 0.088[c]	36.1 ± 0.16[c]
20	40	841	4.59 ± 0.21[d]	5.45 ± 0.00025[d]	0.173 ± 0.0012[d]	14.8 ± 0.12[d]	31.7 ± 0.23[d]
30	40	911	6.73 ± 0.20[e]	7.38 ± 0.00022[e]	0.162 ± 0.0012[e]	14.0 ± 0.12[d]	22.0 ± 0.17[e]
17	35	839	3.81 ± 0.015[c]	4.55 ± 0.000017[f]	0.167 ± 0.00075[f]	14.3 ± 0.075[d]	36.8 ± 0.16[f]
PCL-HA (10M)							
17	35	839	3.81 ± 0.015[c]	4.55 ± 0.000017[f]	0.167 ± 0.0012[g]	13.3 ± 0.90[e,d]	36.5 ± 0.25[f,c]
30	40	911	6.73 ± 0.20[e]	7.38 ± 0.00022[e]	0.145 ± 0.00085[h]	12.7 ± 0.045[f,e]	19.6 ± 0.12[g]
PCL-HA (20M)							
17	35	839	3.81 ± 0.015[c]	4.55 ± 0.000017[f]	0.136 ± 0.0012[i]	12.0 ± 0.042[g,f]	29.9 ± 0.26[h]
30	40	911	6.73 ± 0.20[e]	7.38 ± 0.00022[e]	0.124 ± 0.00085[j]	11.0 ± 0.076[g]	16.8 ± 0.12[i]
PCL-HA (10S)							
17	35	839	3.81 ± 0.015[c]	4.55 ± 0.000017[f]	0.122 ± 0.0012[j]	12.4 ± 0.82[e,f]	26.0 ± 0.26[j]
30	40	911	6.73 ± 0.200[e]	7.38 ± 0.00022[e]	0.126 ± 0.00085[j]	11.2 ± 0.10[g]	17.3 ± 0.12[i]

Values represent the means ± standard deviation; $n = 3$. Means with different superscripts in the same column are significantly different at 0.05 level.

the calculated value of k_H is 0.0379 $(MPa)^{-1}$ which is in very good agreement with the reported value of 0.0342 $(MPa)^{-1}$ obtained by extrapolating the results from CO_2 sorption in PCL experiments on higher temperatures [18].

The most important property of the experimental melting point curve is the location of the abrupt change in the slope. The location of this change, so called "kink" point [18], usually represents the maximum melting point depression of the given compound. Knowing of this temperature is valuable to predict whether a polymer will melt at a sufficiently low temperature to avoid thermal degradation of the active substance which is incorporated (thymol) or just to reduce energy for heating. The kink point is correlated with equivalence of molar volumes of the pure crystal and the pure diluent:

$$V_u^S = V_{CO_2}^V = \frac{ZRTm}{P} \quad (13)$$

where V_u^S and $V_{CO_2}^V$ are molar volumes of the pure crystal (corresponding Kuhn unit) and pure diluent, respectively. When the experimental data on the T_m–P dependency exist, even for the low pressures only, the "kink point" can be estimated from the intersection of the diluent isochor from Eq. (11) with the experimental linear regime or its extrapolation (Fig. 9). Plotting the T_m–P experimental data and fitting the isochor slope to the experimental value of the kink point for the PCL obtained in this study (10 MPa), V_u^S for the neat PCL can be estimated (2.55×10^{-4} m^3/mol). Accordingly, the molecular weight corresponding to the Kuhn unit was calculated (306 Da). The molecular weight of the Kuhn unit corresponds to the Kuhn length which is often used to describe the behavior of the polymers or their blends [76].

3.4. The efficiency of SSI with thymol

Thymol incorporation into the PCL and selected PCL-HA composites by SSI was investigated as a possibility to create antibacterial scaffolds in an environmentally friendly way. The data on sorption kinetics, foam morphology and thermal behavior of the PCL and PCL-HA were considered in choosing adequate pressure and temperature conditions for the SSI. In this study, PCL-HA (10M) and PCL-HA (20M) were chosen for fabrication of antibacterial scaffolds due to the simplicity of the preparation and satisfactory thermal behavior. Sample PCL-HA (10S) was taken into consideration for comparative analysis due to the highest $scCO_2$ solubility and diffusion coefficient observed on both moderately high (17 MPa) and high (30 MPa) pressure. Time of impregnation of 2 h was chosen for two reasons. The first one relates to the highest sorption rates and previous visual observations on plasticizing profile of the PCL at 35–40 °C [20]. The other reason is to minimize negative effects of the higher amount of adsorbed thymol (during longer time of SSI) on foam morphology like previously reported [62].

Experimental data on solubility of thymol in CO_2, thymol fraction in polymer, thymol impregnation yields and partitioning coefficients are given in Table 6.

Satisfactory high SSI yields (11.0–23.7%) were achieved for all the samples in the given pressure range. The efficiency of the SSI of PCL and PCL-HA with thymol was quantified with the partition coefficient, K_c (ratio of the thymol concentration in the polymer and fluid phase). A strong positive correlation was established for $scCO_2$ density and thymol concentration in the gas phase ($r = 0.962$). On the other hand, there was a strong negative correlation between $scCO_2$ density and mass fraction of thymol loaded into the polymer phase ($r = -0.973$). Accordingly, the K_c decreased with the pressure ($scCO_2$ density). This result indicated a higher affinity of thymol to $scCO_2$ than to thepolymer phase at higher pressures (especially above 17 MPa). Lower solvent densities are thus suggested as favorable for the SSI process. Similar phenomena have been recently reported for SSI impregnation of cellulose acetate with thymol [62] and poly(methylmethacrylate-*co*-ethylhexylacrylateco-ethyleneglycoldimethacrylate) with flurbiprofen [77]. A small variation of temperature (35 °C and 40 °C) at 17 MPa seems to have negligible influence on the efficiency of PCL impregnation at 17 MPa (~5%) (Table 6). This was expected given that this temperature difference didn't affect foam

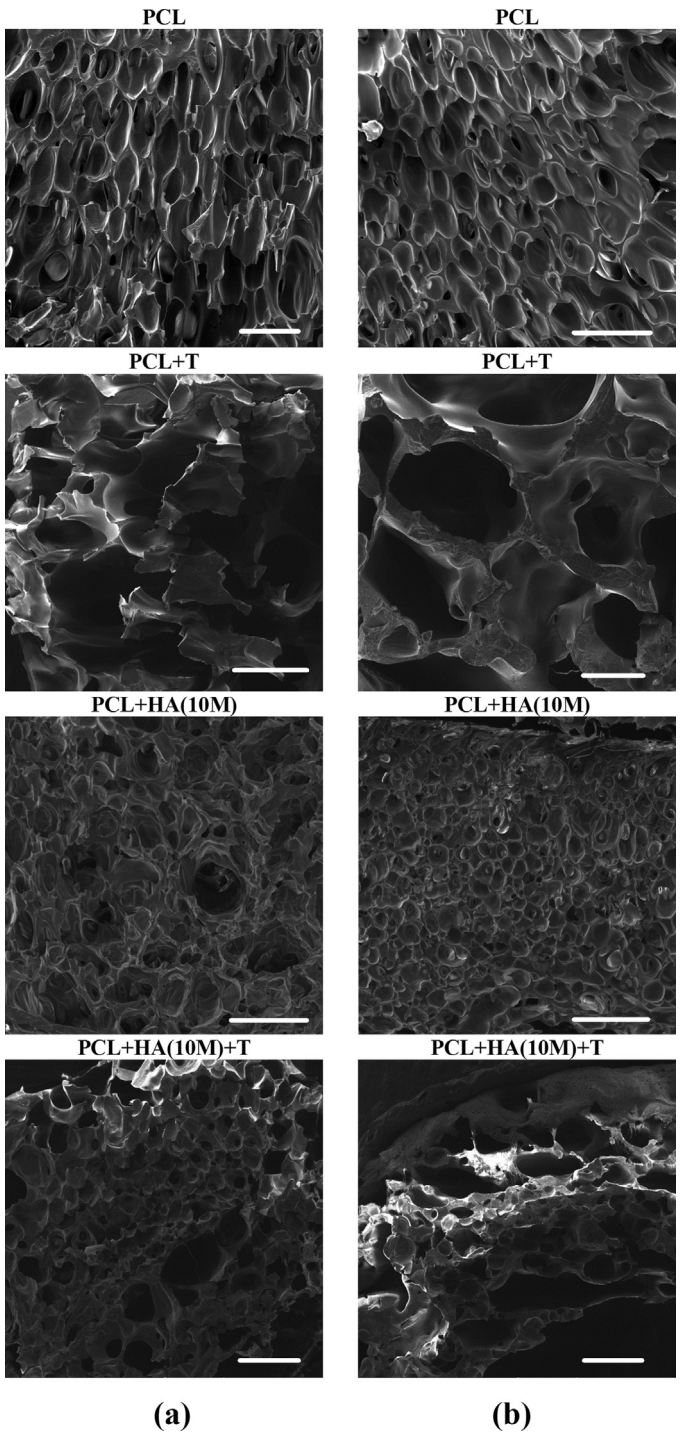

Fig. 10. Influence of the thymol (T) loading on the pore morphology of PCL and PCL-HA (10M) samples at (a) 17 MPa and 35 °C, and (b) 30 MPa and 40 °C (scale bar = 500 μm).

morphology (Table 2). According to the mass transfer analysis presented in Section 3.2, a smaller thymol fraction in the polymer phase (PCL and PCL-HA) could be also due to the lower diffusion of the gas at higher pressures (Tables 3 and 4) due to the prevailing effect of the hydrostatic pressure.

The efficiency of SSI of composites was 7.0–16.4% lower in comparison to impregnation of the virgin polymer at the same conditions (Table 6). As expected, the difference in the SSI efficiency for the composites and neat PCL was more noticeable at the lower pressure, 17 MPa (due to the lower affinity of thymol to the $scCO_2$). The efficiency of PCL-HA (10M) impregnation with thymol was the most similar to neat PCL justifying again the suitability for the further use of this type of composite in the production of functionalized scaffolds. According to the values of K_c, the increased amount of filler (20%) had more pronounced effect on the SSI efficiency than type of HA powder.

The effect of impregnate on the foam morphology was analyzed by SEM. Corresponding SEM images for the representative PCL and PCL-HA samples are given in Fig. 10. As can be seen, PCL-HA (10M) seemed to be more suitable for the SSI with thymol then the neat PCL given that its foam morphology was less affected by the presence of the impregnate, especially at lower pressure (Fig. 10a). The average pore diameters of the composite foam impregnated with thymol at 17 MPa ($198 \pm 73\ \mu m$) and non-impregnated composite foam obtained at the same pressure ($204 \pm 75\ \mu m$, Table 2) were practically the same. Unlikely, average pore diameter of the PCL foam impregnated with thymol at 17 MPa was 54% larger ($455 \pm 95\ \mu m$) than one observed for the non-impregnated PCL foam at the same pressure ($296 \pm 78\ \mu m$, Table 2). The SSI at higher pressure (30 MPa) had more pronounced effect on the PCL-HA (10M) and PCL foam morphology (Fig. 10b). The SSI at 30 MPa resulted in 80% larger pores for PCL-HA (10M) and even 100% larger pores for PCL ($257 \pm 144\ \mu m$ and $621 \pm 347\ \mu m$, respectively) than observed for non-impregnated samples at the same pressure (Table 2).

According to the presented results, moderately high pressures (13–17 MPa) and the low percentage of HA (10%) are suggested for production of PCL scaffolds with satisfying foam microstructure (mean pore diameter of 200–300 μm), even filler distribution and thymol impregnation yields (12–18%). This is due to the satisfactory high $scCO_2$ solubility (0.25–0.30 g/g) and mass transfer rate ($\sim 10^{-10}\ m^2/s$) in the polymer phase as well as the great plasticizing effect ($-\Delta T_m = 26.4–27.4\ ^\circ C$). At pressures above 20 MPa, mass transfer rate and SSI efficiency were negatively affected by higher saturation of the polymer phase with $scCO_2$ (0.30–0.55 g/g), thymol solubility in $scCO_2$ (>5.5 g/kg) and filler amount (20%).

4. Conclusions

In this study the effect of $scCO_2$ in processing of PCL and PCL-HA as the swelling agent, plasticizer and solvent for thymol loading has been analyzed and quantified. A high solubility of $scCO_2$ in PCL and PCL-HA and its effect on the melting peak depression (26–28 °C) suggest possibility of their processing at mild temperatures and moderately high to high pressures (10–30 MPa). The presence of 10% of HA in PCL was advantageous compared to 20% of HA in PCL and virgin PCL regarding the swelling, sorption kinetics, foam morphology and efficiency of the SSI with thymol. The HA powder prepared by the precipitation with mechanical stirring was suggested as favorable due to the simplicity of creation and satisfactory performances regarding swelling, foam morphology, thermal behavior and SSI efficiency (10% in the composite). The high impregnation yields of thymol were achieved after just 2 h of soaking for all the samples (11–23.7%). However, moderate to moderately high pressures (13–17 MPa) and presence of 10% of HA were suggested as favorable for achieving both satisfying impregnation yields of thymol and morphology of PCL foam. For specific biomedical applications, the effect of the thymol amount on mechanical properties of the scaffold and kinetics of thymol release should be further investigated.

Acknowledgements

The authors would like to thank Eurotechnica GmbH (Bargteheide,Germany), TuTech Innovation GmbH and TUHH (Hamburg, Germany) for the financial support and their collaboration in the sorption and HP-DSC measurements. National Research Council (CONICET, Argentina), University of Mar del Plata (Argentina) is gratefully acknowledged for providing the testing material. Financial support from the Ministry of Education, Science and Technological Development of the Republic of Serbia (Project No III45017) is gratefully acknowledged.

References

[1] E.K. Moioli, P.A. Clark, X. Xin, S. Lal, J.J. Mao, Matrices and scaffolds for drug delivery in dental, oral and craniofacial tissue engineering, Adv. Drug. Deliv. Rev. 59 (2007) 308–324.
[2] X. Zhang, W. Chang, P. Lee, Y. Wang, M. Yang, J. Li, S.G. Kumbar, X. Yu, Polymer–ceramic spiral structured scaffolds for bone tissue engineering: effect of hydroxyapatite composition on human fetal osteoblasts, PLoS ONE 9 (2014) 2–11.
[3] K. Kim, C.H. Lee, B.K. Kim, J.J. Mao, Anatomically shaped tooth and periodontal regeneration by cell homing, J. Dent. Res. 89 (2010) 842–847.
[4] X. Yang, F. Yang, X.F. Walboomers, Z. Bian, M. Fan, J.A. Jansen, The performance of dental pulp stem cells on nanofibrous PCL/gelatin/nHA scaffolds, J. Biomed. Mater. Res., A 93 (2010) 247–257.
[5] E. Reverchon, S. Cardea, Supercritical fluids in 3-D tissue engineering, J. Supercrit. Fluids 69 (2012) 97–107.
[6] A.R. Amini, C.T. Laurencin, S.P. Nukavarapu, Bone tissue engineering: recent advances and challenges, Crit. Rev. Biomed. Eng. 40 (2013) 363–408.
[7] M.A. Woodruff, D.W. Hutmacher, The return of a forgotten polymer—polycaprolactone in the 21st century, Prog. Polym. Sci. 35 (2010) 1217–1256.
[8] M. Bhamidipati, A.M. Scurto, M.S. Detamore, The future of carbon dioxide for polymer processing in tissue engineering, Tissue Eng., B 19 (2013) 221–232.
[9] Y. Hayashi, M. Imai, K. Yanagiguchi, I.L. Viloria, T. Ikeda, Hydroxyapatite applied as direct pulp capping medicine substitutes for osteodentin, J. Endod. 25 (1999) 225–229.
[10] S.-J. Heo, S.-E. Kim, J. Wei, Y.-T. Hyun, H.-S. Yun, D.-H. Kim, J.W. Shin, J.-W. Shin, Fabrication and characterization of novel nano- and micro-HA/PCL composite scaffolds using a modified rapid prototyping process, J. Biomed. Mater. Res., A 89 (2009) 108–116.
[11] L. Shor, S. Güçeri, X. Wen, M. Gandhi, W. Sun, Fabrication of three-dimensional polycaprolactone/hydroxyapatite tissue scaffolds and osteoblast–scaffold interactions in vitro, Biomaterials 28 (2007) 5291–5297.
[12] A. Salerno, S. Zeppetelli, E. Di Maio, S. Iannace, P.A. Netti, Novel 3D porous multi-phase composite scaffolds based on PCL, thermoplastic zein and ha prepared via supercritical CO_2 foaming for bone regeneration, Compos. Sci. Technol. 70 (2010) 1838–1846.
[13] V. D'Antò, M.G. Raucci, V. Guarino, S. Martina, R. Valletta, L. Ambrosio, Behaviour of human mesenchymal stem cells on chemically synthesized HA–PCL scaffolds for hard tissue regeneration, J. Tissue Eng. Regen. Med. (2013), http://dx.doi.org/10.1002/term.1768 (xxx xxx).
[14] A. Salerno, M.A. Fanovich, C.D. Pascual, The effect of ethyl-lactate and ethyl-acetate plasticizers on PCL and PCL–HA composites foamed with supercritical CO_2, J. Supercrit. Fluids 95 (2014) 394–406.
[15] M.A. Fanovich, J. Ivanovic, D. Misic, M.V. Alvarez, P. Jaeger, I. Zizovic, R. Eggers, Development of polycaprolactone scaffold with antibacterial activity by an integrated supercritical extraction and impregnation process, J. Supercrit. Fluids 78 (2013) 42–53.
[16] M. Karimi, M. Heuchel, T. Weigel, M. Schossig, D. Hofmann, A. Lendlein, Formation and size distribution of pores in poly(ε-caprolactone) foams prepared by pressure quenching using supercritical CO_2, J. Supercrit. Fluids 61 (2012) 175–190.
[17] M.G. Pastore Carbone, E. Di Maio, G. Scherillo, G. Mensitieri, S. Iannace, Solubility, mutual diffusivity, specific volume and interfacial tension of molten PCL/CO_2 solutions by a fully experimental procedure: effect of pressure and temperature, J. Supercrit. Fluids 67 (2012) 131–138.
[18] Z. Lian, S.A. Epstein, C.W. Blenk, A.D. Shine, Carbon dioxide-induced melting point depression of biodegradable semicrystalline polymers, J. Supercrit. Fluids 39 (2006) 107–117.

[19] S.G. Kazarian, G.G. Martirosyan, Spectroscopy of polymer/drug formulations processed with supercritical fluids: in situ ATR-IR and Raman study of impregnation of ibuprofen into PVP, Int. J. Pharm. 232 (2002) 81–90.
[20] M.A. Fanovich, P. Jaeger, Sorption and diffusion of compressed carbon dioxide in polycaprolactone for the development of porous scaffolds, Mater. Sci. Eng., C 32 (2012) 961–968.
[21] M.M. Hasan, Y.G. Li, G. Li, C.B. Park, P. Chen, Determination of solubilities of CO_2 in linear and branched polypropylene using a magnetic suspension balance and a PVT apparatus, J. Chem. Eng. Data 55 (2010) 4885–4895.
[22] S. Cotugno, E. Di Maio, C. Ciardiello, S. Iannace, G. Mensitieri, L. Nicolais, Sorption thermodynamics and mutual diffusivity of carbon dioxide in molten polycaprolactone, Ind. Eng. Chem. Res. 42 (2003) 4398–4405.
[23] I. Kikic, Polymer–supercritical fluid interactions, J. Supercrit. Fluids 47 (2009) 458–465.
[24] S. Takahashi, J.C. Hassler, E. Kiran, Melting behavior of biodegradable polyesters in carbon dioxide at high pressures, J. Supercrit. Fluids 72 (2012) 278–287.
[25] Y.-M. Wang, X.-B. Lu, Polymeric materials modification with supercritical CO_2 both as a solvent and swelling agent, in: M.R. Belinsky (Ed.), Supercritical Fluids, Nova Science Publishers, Inc, Hauppauge NY, 2010, pp. 667–687.
[26] S.C. Frerich, Biopolymer foaming with supercritical CO_2—thermodynamics, foaming behaviour and mechanical characteristics, J. Supercrit. Fluids 96 (2015) 349–358.
[27] C. Gutiérrez, J.F. Rodríguez, I. Gracia, A. de Lucas, M.T. García, Development of a strategy for the foaming of polystyrene dissolutions in $scCO_2$, J. Supercrit. Fluids 76 (2013) 126–134.
[28] J.M.S. Fonseca, R. Dohrn, S. Peper, High-pressure fluid-phase equilibria: experimental methods and systems investigated (2005–2008), Fluid Phase Equilib. 300 (2011) 1–69.
[29] M.Z. Hossain, A.S. Teja, Modeling phase equilibria in CO_2 + polymer systems, J. Supercrit. Fluids 96 (2015) 313–323.
[30] E. Di Maio, G. Mensitieri, S. Iannace, L. Nicolais, W. Li, R.W. Flumerfelt, Structure optimization of polycaprolactone foams by using mixtures of CO_2 and N_2 as blowing agents, Polym. Eng. Sci. 45 (2005) 432–441.
[31] Y.-T. Shieh, H.-S. Yang, Morphological changes of polycaprolactone with high-pressure CO_2 treatment, J. Supercrit. Fluids 33 (2005) 183–192.
[32] F. Dreisbach, H.W. Lösch, Magnetic suspension balance for simultaneous measurement of a sample and the density of the measuring fluid, Therm. Anal. Calorim. 62 (2000) 515–521.
[33] E. Aionicesei, M. Škerget, Ž. Knez, Solubility and diffusivity of supercritical CO_2 in bioresorbable polymers: measurements, calculations and potential applications in polymer foaming, in: 12th European Meeting on Supercritical Fluids, ISASF, International Society for Advancement of Supercritical Fluids, Graz, 2010, pp. 1–10.
[34] E. De Paz, S. Rodrı, J. Herreras, Determination of phase equilibrium (solid–liquid–gas) in poly-(ε-caprolactone)-carbon dioxide systems, J. Chem. Eng. Data 55 (2010) 2781–2785.
[35] A. Salerno, E. Di Maio, S. Iannace, P.A. Netti, Solid-state supercritical CO_2 foaming of PCL and PCL-HA nano-composite: effect of composition, thermal history and foaming process on foam pore structure, J. Supercrit. Fluids 58 (2011) 158–167.
[36] M.J. Jenkins, K.L. Harrison, M.M.C.G. Silva, M.J. Whitaker, K.M. Shakesheff, S.M. Howdle, Characterisation of microcellular foams produced from semi-crystalline PCL using supercritical carbon dioxide, Eur. Polym. J. 42 (2006) 3145–3151.
[37] E. Kiran, K. Liu, K. Ramsdell, Morphological changes in poly(ε-caprolactone) in dense carbon dioxide, Polymer 49 (2008) 1853–1859.
[38] Y.P. Handa, S. Lampron, M.L. O'neill, On the plasticization of poly(2,6-dimethyl phenylene oxide) by CO_2, J. Polym. Sci., B: Polym. Phys. 32 (1994) 2549–2553.
[39] M. Takada, S. Hasegawa, M. Ohshima, Crystallization kinetics of poly(L-lactide) in contact with pressurized CO_2, Polym. Eng. Sci. 44 (2004) 186–196.
[40] M.K. Hrnčič, E. Markočič, N. Trupej, M. Škerget, Ž. Knez, Investigation of thermodynamic properties of the binary system polyethylene glycol/CO_2 using new methods, J. Supercrit. Fluids 87 (2014) 50–58.
[41] Y. Paul, Z. Zhang, Y.P. Handa, High-pressure calorimetric study of plasticization of poly(methyl methacrylate) by methane, ethylene, and carbon dioxide, J. Polym. Sci., B: Polym. Phys. 36 (1998) 977–982.
[42] J. Reignier, R. Gendron, M.F. Champagne, Autoclave foaming of poly(ε-caprolactone) using carbon dioxide: impact of crystallization on cell structure, J. Cell. Plast. 43 (2007) 459–489.
[43] V. Sedlarik, Antimicrobial modifications of polymers, in: R. Chamy, F. Rosenkranz (Eds.), Biodegradation—Life of Science, InTech, Croatia, 2013, pp. 187–204.
[44] P.A. Stone, P.A. Armstrong, D.F. Bandyk, R.S. Brumberg, S.K. Flaherty, M.R. Back, B.L. Johnson, M.L. Shames, Use of antibiotic-loaded polymethylmethacrylate beads for the treatment of extracavitary prosthetic vascular graft infections, J. Vasc. Surg. 44 (2006) 757–761.
[45] H.-W. Kim, J. Knowles, H.-E. Kim, Hydroxyapatite porous scaffold engineered with biological polymer hybrid coating for antibiotic Vancomycin release, J. Mater. Sci.: Mater. Med. 16 (2005) 189–195.
[46] D. Puppi, D. Dinucci, C. Bartoli, C. Mota, C. Migone, F. Dini, G. Barsotti, F. Carlucci, F. Chiellini, Development of 3D wet-spun polymeric scaffolds loaded with antimicrobial agents for bone engineering, J. Bioac. Compat. Polym. 26 (2011) 478–492.
[47] X. Liu, Q. Feng, A. Bachhuka, K. Vasilev, Surface modification by allylamine plasma polymerization promotes osteogenic differentiation of human adipose-derived stem cells, Appl. Surf. Sci. 6 (2014) 9733–9741.
[48] A. Wattanasatcha, S. Rengpipat, S. Wanichwecharungruang, Thymol nanospheres as an effective anti-bacterial agent, Int. J. Pharm. 434 (2012) 360–365.
[49] A. Nostro, A.R. Blanco, M.A. Cannatelli, V. Enea, G. Flamini, I. Morelli, A. Sudano Roccaro, V. Alonzo, Susceptibility of methicillin-resistant staphylococci to oregano essential oil, carvacrol and thymol, FEMS Microbiol. Lett. 230 (2004) 191–195.
[50] S. Cosentino, C.I. Tuberoso, B. Pisano, M. Satta, V. Mascia, E. Arzedi, F. Palmas, *In-vitro* antimicrobial activity and chemical composition of Sardinian *Thymus* essential oils, Lett. Appl. Microbiol. 29 (1999) 130–135.
[51] I. Kruk, T. Michalska, K. Lichszteld, A. Kładna, H.Y. Aboul-Enein, The effect of thymol and its derivatives on reactions generating reactive oxygen species, Chemosphere 41 (2000) 1059–1064.
[52] R. Aeschbach, J. Löliger, B.C. Scott, A. Murcia, J. Butler, B. Halliwell, O.I. Aruoma, Antioxidant actions of thymol, carvacrol, 6-gingerol, zingerone and hydroxytyrosol, Food Chem. Toxicol. 32 (1994) 31–36 (An International Journal Published for the British Industrial Biological Research Association).
[53] K.R. Riella, R.R. Marinho, J.S. Santos, R.N. Pereira-Filho, J.C. Cardoso, R.L.C. Albuquerque-Junior, S.M. Thomazzi, Anti-inflammatory and cicatrizing activities of thymol, a monoterpene of the essential oil from *Lippia gracilis*, in rodents, J. Ethnopharmacol. 143 (2012) 656–663.
[54] S. Shapiro, B. Guggenheim, The action of thymol on oral bacteria, Oral Microbiol. Immunol. 10 (1995) 241–246.
[55] D. Yu, S.K. Pearson, W.H. Bowen, D. Luo, B.E. Kohut, D.S. Harper, Caries inhibition efficacy of an antiplaque/antigingivitis dentifrice, Am. J. Dent. 13 (2000) 14C–17C.
[56] Y. Takeuchi, B. Guggenheim, A. Filieri, B.P. Effect, A. Filieri, Effect of chlorhexidine/thymol and fluoride varnishes on dental biofilm formation *in vitro*, Eur. J. Oral Sci. 115 (2007) 468–472.
[57] S. Milovanovic, M. Stamenic, D. Markovic, M. Radetic, I. Zizovic, Solubility of thymol in supercritical carbon dioxide and its impregnation on cotton gauze, J. Supercrit. Fluids 84 (2013) 173–181.
[58] A.M.A. Dias, M.E.M. Braga, I.J. Seabra, P. Ferreira, M.H. Gil, H.C. de Sousa, Development of natural-based wound dressings impregnated with bioactive compounds and using supercritical carbon dioxide, Int. J. Pharm. 408 (2011) 9–19.
[59] A. Torres, J. Romero, A. Macan, A. Guarda, M.J. Galotto, Near critical and supercritical impregnation and kinetic release of thymol in LLDPE films used for food packaging, J. Supercrit. Fluids 85 (2014) 41–48.
[60] S. Milovanovic, I. Jankovic-Castvan, J. Ivanovic, I. Zizovic, Effect of starch xero- and aerogels preparation on the supercritical CO_2 impregnation of thymol, Starch 67 (2015) 174–182.
[61] J. Ivanovic, S. Milovanovic, M. Stamenic, M.A. Fanovich, P. Jaeger, I. Zizovic, Application of an integrated supercritical extraction and impregnation process for incorporation of thyme extracts into different carriers, in: J. Osborne (Ed.), Handbook on Supercritical Fluids: Fundamentals, Properties and Applications, Nova Science Publishers, Inc, Hauppauge, NY, 2014, pp. 257–280.
[62] S. Milovanovic, M. Stamenic, D. Markovic, J. Ivanovic, I. Zizovic, Supercritical impregnation of cellulose acetate with thymol, J. Supercrit. Fluids 97 (2015) 107–115.
[63] M.A. Giardina, M.A. Fanovich, Synthesis of nanocrystalline hydroxyapatite from $Ca(OH)_2$ and H_3PO_4 assisted by ultrasonic irradiation, Ceram. Int. 36 (2010) 1961–1969.
[64] A. López-Macipe, J. Gómez-Morales, R. Rodríguez-Clemente, Nanosized hydroxyapatite precipitation from homogeneous calcium/citrate/phosphate solutions using microwave and conventional heating, Adv. Mater. 10 (1998) 49–53.
[65] J. von Schnitzler, R. Eggers, Mass transfer in polymers in a supercritical CO_2-atmosphere, J. Supercrit. Fluids 16 (1999) 81–92.
[66] J. Crank, The Mathematics of Diffusion, second ed., Oxford University Press, Ely House, London W.I, 1975.
[67] S. Areerat, E. Funami, Y. Hayata, D. Nakagawa, M. Ohshima, Measurement and prediction of diffusion coefficients of supercritical CO_2 in molten polymers, Polym. Eng. Sci. 44 (2004) 1915–1924.
[68] Q. Xu, X. Ren, Y. Chang, J. Wang, L. Yu, K. Dean, Generation of microcellular biodegradable polycaprolactone foams in supercritical carbon dioxide, J. Appl. Polym. Sci. 94 (2004) 593–597.
[69] S. Jiang, X. Ji, L. An, B. Jiang, Crystallization behavior of PCL in hybrid confined environment, Polymer 42 (2001) 3901–3907.
[70] E. Markočič, M. Škerget, Ž. Knez, Solubility and diffusivity of CO_2 in poly(L-lactide)–hydroxyapatite and poly(D,L-lactide-*co*-glycolide)–hydroxyapatite composite biomaterials, J. Supercrit. Fluids 55 (2011) 1046–1051.
[71] J.R. Jones, New trends in bioactive scaffolds: the importance of nanostructure, J. Eur. Ceram. Soc. 29 (2009) 1275–1281.
[72] E. Aionicesei, M. Škerget, Ž. Knez, Measurement of CO_2 solubility and diffusivity in poly(L-lactide) and poly(D,L-lactide-*co*-glycolide) by magnetic suspension balance, J. Supercrit. Fluids 47 (2008) 296–301.

[73] A.R. Manninen, H.E. Naguib, A.V. Nawaby, M. Day, CO_2 sorption and diffusion in polymethyl methacrylate–clay nanocomposites, Polym. Eng. Sci. 45 (2005) 904–914.
[74] Ž. Knez, M. Škerget, Z. Mandžuka, Determination of S–L phase transitions under gas pressure, J. Supercrit. Fluids 55 (2010) 648–652.
[75] E. Weidner, V. Wiesmet, Z. Knez, M. Skerget, Phase equilibrium (solid–liquid–gas) in polyethyleneglycol–carbon dioxide systems, J. Supercrit. Fluids 10 (1997) 139–147.
[76] J.D. Hoffman, R.L. Miller, Kinetic of crystallization from the melt and chain folding in polyethylene fractions revisited: theory and experiment, Polymer 38 (1997) 3151–3212.
[77] A.R.C. Duarte, A.L. Simplicio, A. Vega-González, P. Subra-Paternault, P. Coimbra, M.H. Gil, H.C. de Sousa, C.M.M. Duarte, Supercritical fluid impregnation of a biocompatible polymer for ophthalmic drug delivery, J. Supercrit. Fluids 42 (2007) 373–377.